Journal of Scientific Computing (2021) 87:50
https://doi.org/10.1007/s10915-021-01469-0

The Role of Boundary Conditions on Convergence Properties of Peridynamic Model for Transient Heat Transfer

Tie Mei[1] · Jiangming Zhao[3] · Zian Liu[1] · Xuhao Peng[1] · Ziguang Chen[1,2] · Florin Bobaru[3]

Received: 13 November 2019 / Revised: 11 January 2021 / Accepted: 19 March 2021

Abstract
Normally, peridynamic (PD) models for transient heat transfer converge, in the limit of the horizon size going to zero, to the solution of the corresponding PDE-based heat transfer. However, different ways of imposing local boundary conditions have been observed to lead to some interesting properties that may deliver the classical solution at a point in space and time from a series of PD solutions obtained with relatively large horizons. Here, we use analytical derivation of PD solutions to explain how approximations introduced by the one-point Gaussian discretization in space (the so-called "meshfree" PD method) and by specific implementations of boundary conditions lead to the intersection of m-convergence curves at the exact value of the corresponding classical model solution. This leads to a strategy of approximating the local solution better with a sequence of PD models that use relatively large horizons compared to a PD model that uses a small horizon. We analyze this property for transient heat conduction in homogeneous and heterogeneous bars. We find that material interfaces influence the intersection of m-convergence curves for transient heat conduction in a 1D heterogeneous bar.

Keywords Peridynamics · Asymptotically compatible scheme · Nonlocal diffusion · Convergence · Transient diffusion · Boundary conditions

1 Introduction

Most heat transfer processes at the macro-scale can be well represented by a local model based on Fourier's law. However, nonlocal effects are not negligible in low temperature environments, short-pulse-laser heating, heat transport with steep temperature gradients,

✉ Ziguang Chen
zchen@hust.edu.cn

[1] Department of Engineering Mechanics, School of Aerospace Engineering, Huazhong University of Science and Technology, Wuhan 430074, China

[2] Hubei Key Laboratory of Engineering Structural Analysis and Safety Assessment, 1037 Luoyu Road, Wuhan 430074, China

[3] Department of Mechanical and Materials Engineering, University of Nebraska-Lincoln, Lincoln, NE 68588-0526, USA

Published online: 31 March 2021

and most heat transport processes at the micro- and nano-scales. Motivated by such effects, several nonlocal heat transfer theories have been proposed [1–8]. An area where the aforementioned nonlocal models cannot be directly applied is the set of problems with discontinuities in the system emerging, interacting, and evolving.

The peridynamic (PD) theory, originally introduced by Stewart Silling [9, 10], is increasingly gaining attention from both academia and industry. The PD formulation is an integro-differential-type model, based on nonlocal interactions between material points in a continuum. It allows spatial discontinuities to be treated as natural parts of the solution process, which is particularly well suited for dealing with cracks and damage in solid mechanics, especially in situations where the crack path is not known in advance [11]. Driven by nonlocal diffusion problems, Gerstle et al. [12], Bobaru and Duangpanya [13], extended the ideas of Silling to diffusion, and formulated a PD model for transient heat conduction in bodies with evolving discontinuities [14]. These models use the bond-based version of peridynamics. Generic forms of PD diffusion models have recently been analyzed mathematically as well [15, 16]. Recently, state-based peridynamic heat conduction models have been introduced to consider the non-Fourier heat transfer and nonlocal effects [17], or coupled thermomechanics problems [18]. The limitation of a fixed Poisson's ratio is the main reason for the state-based extension of bond-based PD theory in mechanical problems. Diffusion problems are single-parameter problems, and have no such limitation. In this paper, we focus on the convergence behavior of bond-based PD model of transient heat diffusion.

In our previous work [19, 20], we analyzed the convergence behavior of the PD numerical solution with the one-point Gaussian spatial integration method (or the "meshfree" PD discretization) for transient diffusion and elasticity. The one-point Gauss quadrature is the preferred method for discretizing PD models because it leads to a meshfree model, very well suited for capturing the evolution of fracture and damage (or other types of discontinuities) in a material (see e.g. [14] and [21]). The results in [19, 20] showed that only the integrand from the constructive approach, leads to results that converge to the classical solution in the limit of the horizon going to zero when the relative grid-density m (the ratio between the horizon size and grid spacing) is kept constant (the so-called "δ-convergence") [13]. In the case of transient diffusion, δ-convergence to the classical solution was observed to be monotonic (as the horizon decreases, the difference between the nonlocal solution and the classical one decreases monotonically), based on observations at several points in space and time [19]. We also noticed that due to the finite speed of wave propagation and wave dispersion, δ-convergence for dynamic elasticity is not monotonic, in general [20]. These behaviors observed for the one-point Gaussian quadrature may be more general and persist for other types of discretization, but this remains to be seen.

As a result from the observed monotonic δ-convergence, an interesting behavior of the peridynamic numerical solutions for transient diffusion problems was discovered in [13, 19]: when two "m-convergence"(taking m to go to infinity for a fixed horizon size δ) intersect, the temperature value at the intersection point is also the value of the exact classical solution, when a particular way of implementing the local boundary conditions in a PD model is employed [19]. The crossing of m-convergence curves with the classical solution was attributed to the "competition" among the way boundary conditions are imposed, the peridynamic surface effect, and nonlocality [19].

In a PD simulation, the horizon size is never zero, but one can analyze δ-convergence, in which separate PD simulations are performed using smaller and smaller horizon sizes. The reason for the intersecting point of the m-convergence curves (obtained for different horizon sizes) being the classical solution is as follows: for the cases discussed in [19] (1D transient heat diffusion, subject to Dirichlet boundary conditions imposed on the end

nodes only), for a given horizon size, when the horizon factor is small, the numerical error introduced by the boundary conditions implementation is large; this leads to, for example, temperature values (at a point in time and space) below the corresponding ones from the classical solution; when the horizon factor m increases (tends to infinity, for m-convergence tests), the difference between the PD solution and the classical solution is dominated by the nonlocality and the surface effect (when imposing Dirichlet boundary conditions on the end nodes only); this tend to lead to temperature values above the corresponding ones from the classical solution. In this transition, the m-convergence curves have to cross each other at the same point and the temperature value at that intersection point has to be the classical value, because otherwise would contradict the monotonic δ-convergence property. In other words, under certain conditions, to be explored in the present work, there is a certain m-value for which the solution at a certain point in time and space of the nonlocal problem (even with a large horizon size!) exactly matches the classical value [19].

The conclusion that δ-convergence is monotonic in the case of transient diffusion [19], was reached based on numerical tests. Recently, we have shown how to obtain analytical solutions to the peridynamic models for transient diffusion in 1D and simple 2D domains [22]. Here, we use such analytical solutions to provide a thorough explanation for the previously observed δ-convergence behavior. We discuss how different methods for imposing local boundary conditions affect the crossing of the m-convergence curves at the classical location, and provide requirements that need to be satisfied to have monotonic δ-convergence to the classical solution and the intersection of the m-convergence curves.

This intersection of m-convergence curves at the classical solution value opens the possibility of computing exact classical solutions (at a certain point and time) by solving a set of corresponding nonlocal models with "large" horizons. Normally, local solutions are approximated by nonlocal models in the limit of horizon going to zero. This is interesting in and of itself, and it could even be made practical if, for certain cases, the nonlocal solutions end up being cheaper to compute than computing the local solution. Note that, in general, this works the other way around: nonlocal computations are more expensive than corresponding local ones. Indeed, finding a good approximation of a local model with a corresponding nonlocal one, usually requires a very small nonlocal region (horizon size) and, therefore, a very fine (therefore expensive) discretization. This is the δ-convergence result [13]. The intersection of m-convergence curves, however, points to the possibility of using PD solutions with large horizons (and, thus, relatively coarse spatial discretizations) to deliver the exact solution of the local model, at a specific point in time and space. In this paper, we investigate how the intersection property of the m-convergence curves is affected by the time-step size and the location where the solution is computed at. In addition, while the convergence behavior of the nonlocal model to the classical model has been investigated in [13, 14, 19] only for the homogeneous domain case, here we also consider the case of a heterogeneous bar and the influence of material interfaces on recovering the exact solution of the local model based on computing several corresponding nonlocal models with relatively large horizon sizes.

The paper is organized as follows: we first revisit the convergence behavior for the PD model for transient heat transfer in 1D and, using some new analytical solutions for the nonlocal model, we explain the influence of the way local boundary conditions are imposed on the monotonicity of δ-convergence of PD models to the classical model; in Sect. 3, we discuss how δ-convergence monotonicity affects the intersecting property for the m-convergence curves; in Sect. 4 we study the dependence of the intersecting point m-value on the particular location in time and space where the solution is computed and show the advantage of using the strategy of computing several PD models with large horizons to obtain the

exact solution of the local model; in Sect. 5 we test the intersecting m-convergence curves strategy for transient heat transfer in a heterogeneous bar. Conclusions and future work are presented in Sect. 6. Since heat transfer and mass diffusion problems are mathematically identical, the results in this paper apply directly to mass diffusion problems as well.

2 Monotonicity of δ-Convergence for PD Models of Transient Diffusion in 1D

We first review the PD model for heat transfer in a 1D studied in [13, 19]. Then, using the analytical solution obtained via separation of variables for the PD model, recently introduced in [22], we analyze monotonicity of δ-convergence (of PD solutions to the classical one) in terms of horizon size, for the mirror-type implementation of the Dirichlet boundary conditions. This will help us explain the observed behavior for the m-convergence curves and the dependence of the intersection point of the m-convergence curves on the particular way local boundary conditions are enforced, the horizon size, and the time step size.

Diffusion phenomenon have been described via parabolic-type PDEs, and such models have an infinite propagation speed of heat [23], or via hyperbolic-type PDEs, which lead to a finite propagation speed of heat. For instance, the propagation speeds corresponding to the diffusion equations in [24] and [25] have as limits the sound speed and light speed, respectively. In this paper, we focus on the most common diffusion equation, the parabolic-type.

We first revisit the convergence behavior of 1D PD transient diffusion in a homogeneous bar, with Dirichlet boundary conditions imposed via mirror-type option. The PD diffusion model has the following form:

$$\frac{\partial T(\boldsymbol{x},t)}{\partial t} = \int_{\mathrm{H}_x} J_n\big(\hat{\boldsymbol{x}},\boldsymbol{x},t\big)dV_{\hat{\boldsymbol{x}}} \tag{1}$$

where $T(\boldsymbol{x}, t)$ is the temperature (or concentration in the mathematically-equivalent mass transfer problems) at point $\boldsymbol{x}$ at time t. The region of nonlocal interactions for point $\boldsymbol{x}$, $H_{\boldsymbol{x}}$, is called the horizon region of material point $\boldsymbol{x}$. The thermal bond between $\boldsymbol{x}$ and $\hat{\boldsymbol{x}}$ is characterized by a diffusivity-like quantity $k(||\hat{\boldsymbol{x}} - \boldsymbol{x}||)$, sometimes refer to as the "micro- diffusivity" [13, 14]. The integrand is usually taken to be of the form [13, 26–28]:

$$J_n\big(\hat{\boldsymbol{x}},\boldsymbol{x},t\big) = \begin{cases} k\big(\|\hat{\boldsymbol{x}} - \boldsymbol{x}\|\big)\frac{T(\hat{\boldsymbol{x}},t)-T(\boldsymbol{x},t)}{\|\hat{\boldsymbol{x}}-\boldsymbol{x}\|^n}, \|\hat{\boldsymbol{x}} - \boldsymbol{x}\| \le \delta \\ 0, \|\hat{\boldsymbol{x}} - \boldsymbol{x}\| > \delta \end{cases} \tag{2}$$

where δ is the horizon size (in 1D, δ is half the length of the interval $\mathrm{H}_{\boldsymbol{x}}$; in 2D, δ is the radius of the disk $\mathrm{H}_{\boldsymbol{x}}$ centered at $\boldsymbol{x}$, for a circular choice of the horizon region). Here n is an integer, normally selected to be 0, 1, or 2 (see [13, 14, 28]).

Reference [19] showed that, when the one-point Gauss quadrature is applied, only the integrand from the constructive approach with $n=2$, leads to results that converge to the classical solution in the limit of the horizon going to zero when the relative grid-density m is kept constant. In the rest of the paper we focus on the integrand with $n=2$.

The micro-diffusivity function $k(||\hat{\boldsymbol{x}} - \boldsymbol{x}||)$ can have different profiles, leading to different horizon-scale response, but similar macro-scale behavior. Two popular choices are the "constant" micro-diffusivity (independent of the bond length) and the linear (also called "triangular") micro-diffusivity. Although here, for simplicity, we only use the constant

profile, similar results and conclusions should be obtained with the linear (or other profile) micro-diffusivity. With the linear micro-diffusivity, the PD solution converges to the classic solution faster, as shown in [19]. For the "constant" micro-diffusivity, we have:

$$k\left(\|\hat{\boldsymbol{x}}-\boldsymbol{x}\|\right)=k_0 \tag{3}$$

By matching the PD solution with the classical one for the case of a linear temperature profile, one obtains the following results: $k_0=\frac{K}{\delta}$ in 1D; $k_0=\frac{4K}{\pi\delta^2}$ in 2D; and $k_0=\frac{9K}{2\pi\delta^3}$ in 3D. K is the material diffusivity.

Similar to [19], we consider the example of heat transfer in a 1D homogeneous bar, subject to Dirichlet boundary conditions. In this problem, the length of the bar L is 10 cm, and thermal diffusivity $K=10$ cm^2/s. The initial temperature imposed on the bar is T(x, 0) = 100 °C, $(0<x<L)$. We apply the local-type boundary condition by keeping the boundary temperature $T(0,t)=T(L,t)=0$. The classical diffusion model of this problem is:

$$\begin{cases}\frac{\partial T_c(x,t)}{\partial t}=K\nabla^2 T_c(x,t)\\ T_c(x,0)=100^{\circ}\mathrm{C}, 0<x<L\\ T_c(0,t)=T_c(L,t)=0^{\circ}\mathrm{C}, t>0\end{cases} \tag{4}$$

where $T_c(x,t)$ is the exact solution to this local boundary value problem. Using separation of variables, for example, T_c is found to be [29]:

$$T_c(x,t)=\sum_{i=1,3,5\ldots}^{\infty}\frac{4\theta_o}{i\pi}\sin k_i x\exp\left(-Kk_i{}^2t\right) \tag{5}$$

where $\theta_o=100$ °C and $k_i=\frac{i\pi}{L}$. Figure 1 shows the exact classical solutions to the 1D heat transient problem in the bar, at two time instances: 0.1 s and 0.5 s.

There can be several PD forms (Eq. 1) corresponding to the PDE-based formulation in Eq. (4), depending on the peridynamic kernel one chooses. Moreover, the imposition of local boundary conditions in PD can also take different forms. For example, to impose the local (Dirichlet) boundary condition in the PD model, three possible options are shown in Fig. 2, the first two belonging to the class of "fictitious nodes methods": mirror-type (temperature field in the fictitious domain is related by mirror symmetry to the corresponding

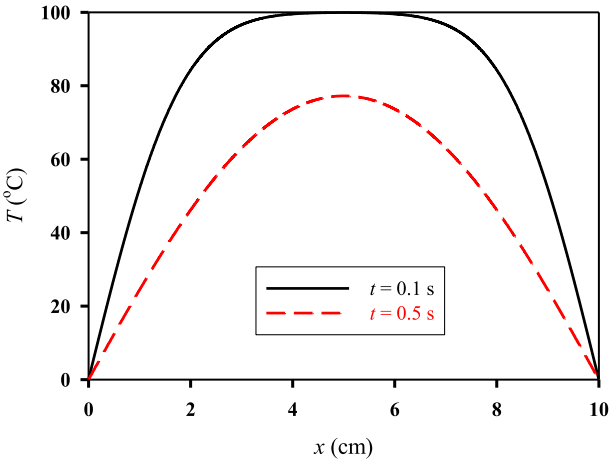

Fig. 1 The exact classical solution for the temperature distribution in a 1D homogeneous bar subject to Dirichlet boundary conditions, at two different times

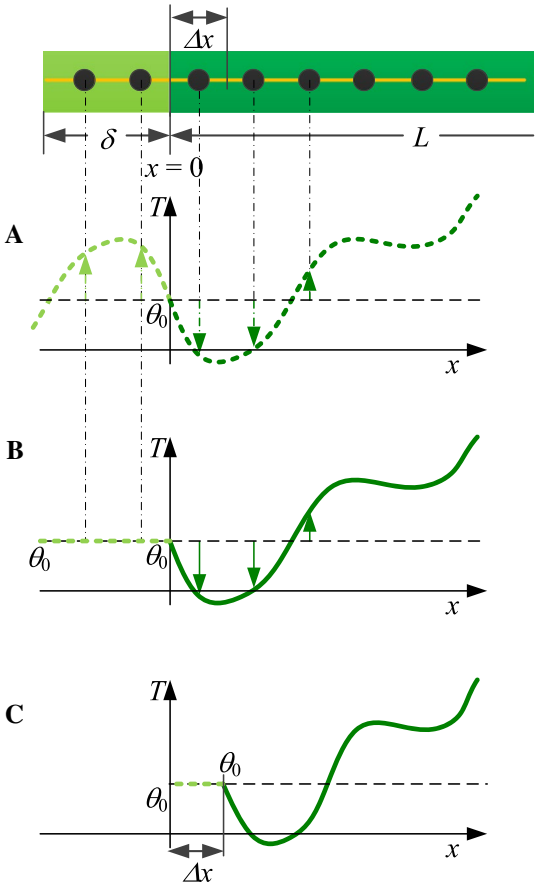

Fig. 2 Three types of imposing Dirichlet boundary conditions in a 1D PD model: **a** mirror-type, **b** naïve-type, and **c** inner-type

domain in the bar, see Fig. 2a), naïve-type (temperature field in the fictitious layer is constant and equal to the value of the local Dirichlet condition, see Fig. 2b), and inner-type (temperature field in a finite layer **inside** the domain is fixed to be the local boundary temperature, see Fig. 2c). While there is a single problem defined by the PD equation and the local boundary conditions we aim to enforce, these different implementations of such conditions could correspond, in general, to slightly different nonlocal problems: the PD equation and different associated nonlocal boundary conditions (or "volume constraints"). This means that for a fixed horizon, taking m to go to infinity (m-convergence) in solving the PD equation with the local B.C. imposed using one of the options above could reach slightly different nonlocal solutions.

We recently showed that the PD equation (Eq. (1)) with the mirror-type boundary conditions has an analytical solution in 1D and in simple domains in 2D ([22]). The PD exact solution for the problem shown in Eq. (4) is [22]:

$$T_{\mathrm{pd}}(x,t) = \sum_{i=1,3,5\ldots}^{\infty} \frac{4\theta_o}{i\pi} \sin k_i x \exp\left(-KA\left(k_i\delta\right)k_i{}^2 t\right) \tag{6}$$

where

$$A\left(k_i\delta\right) = \frac{2\left[\mathrm{Si}\left(k_i\delta\right) + \frac{\cos\left(k_i\delta\right)-1}{k_i\delta}\right]}{k_i\delta} \tag{7}$$

and Si is the sine integral function, defined as $\mathrm{Si}(x) = \int_0^x \frac{\sin z}{z}\mathrm{d}z$. As shown in Fig. 3a, the nonlocal factor, $A\left(k_m\delta\right)$, approaches 1 when δ goes to zero, which confirms that the PD solution $T_{\mathrm{pd}}(x,t)$ converges to the classical solution when the horizon goes to zero.

In [19], based on numerical tests, it was observed that at certain points in space and time δ-convergence can be monotonic (the PD solution, at a point in time and space, for a smaller horizon is closer to the classical solution than for a larger horizon) in the case of transient diffusion. To more fully understand that behavior, we compute the derivative of the analytical PD solution with respect to the horizon size. When the derivative is positive, δ-convergence is monotonic and happens from above (values larger than the classical value), while when the derivative is negative, it is still monotonic but happens from below.

Taking the derivative with respect to the horizon size in Eq. (6), we obtain:

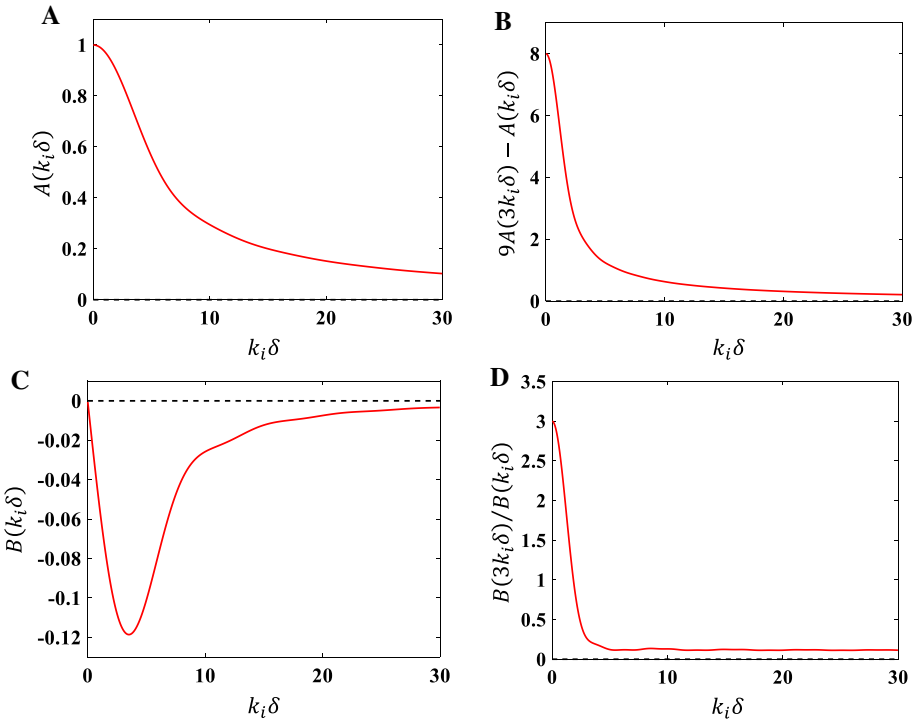

Fig. 3 The dependency of the "nonlocal factor" and other parameters in the analytical PD solution on $k_i\delta$

$$\frac{\partial T_{\mathrm{pd}}(x,t)}{\partial \delta} = \sum_{i=1,3,5\ldots}^{\infty} \frac{4\theta_o}{i\pi}\left(-KB\left(k_i\delta\right){k_i}^3 t\right)\sin k_i x \exp\left(-KA\left(k_i\delta\right){k_i}^2 t\right) \tag{8}$$

where

$$B\left(k_i\delta\right) = \frac{\mathrm{d}A\left(k_i\delta\right)}{\mathrm{d}\left(k_i\delta\right)} = \frac{4 - 4\cos\left(k_i\delta\right) - 2\left(k_i\delta\right)\mathrm{Si}\left(k_i\delta\right)}{\left(k_i\delta\right)^3} \tag{9}$$

Figure 3c shows $B\left(k_i\delta\right)$ is always negative for any non-zero horizon size ($k_i > 0$). The monotonicity of δ-convergence requires the derivative (Eq. 8) to not change sign for any horizon size.

To see whether the time at which the solution is computed influences the sign of the derivative above, we look at large times, when the first term in the series becomes dominant. The ratio of the absolute values between the second and first terms in Eq. (8) is:

$$r = \frac{\left|B\left(k_3\delta\right){k_3}^3 \sin\left(k_3 x\right)\exp\left(-KA\left(k_3\delta\right){k_3}^2 t\right)/3\right|}{\left|B\left(k_1\delta\right){k_1}^3 \sin\left(k_1 x\right)\exp\left(-KA\left(k_1\delta\right){k_1}^2 t\right)\right|} = \frac{\left|9B\left(3k_1\delta\right)\sin\left(3k_1 x\right)\exp\left(-9KA\left(3k_1\delta\right){k_1}^2 t\right)\right|}{\left|B\left(k_1\delta\right)\sin\left(k_1 x\right)\exp\left(-KA\left(k_1\delta\right){k_1}^2 t\right)\right|} \tag{10}$$

Since $\frac{\left|\sin\left(3k_1 x\right)\right|}{\left|\sin\left(k_1 x\right)\right|} \le 3$ and $0 < \frac{B\left(3k_1\delta\right)}{B\left(k_1\delta\right)} \le 3$ (see Fig. 3d), we have:

$$r \le 81\exp\left(-K{k_1}^2 t\left(9A\left(3k_1\delta\right) - A\left(k_1\delta\right)\right)\right) \tag{11}$$

where $0 < 9A\left(3k_1\delta\right) - A\left(k_1\delta\right) \le 8$ (see Fig. 3b). When t is large enough, e.g. $t \ge \frac{10}{K{k_1}^2\left(9A\left(3k_1\delta\right) - A\left(k_1\delta\right)\right)}$, r is much smaller than 1 and the first term in Eq. (8) dominates the sum of the rest of the terms. Therefore, the following approximation holds:

$$\begin{aligned}\frac{\partial T_{\mathrm{pd}}(x,t)}{\partial \delta} &\approx \frac{4\theta_o}{\pi}\left(-KB\left(\frac{\pi}{L}\delta\right)\left(\frac{\pi}{L}\right)^3 t\right)\sin\left(\frac{\pi x}{L}\right)\exp\left(-KA\left(\frac{\pi}{L}\delta\right)\left(\frac{\pi}{L}\right)^2 t\right) > 0 \, for \, t \\ &\ge \frac{10}{K{k_1}^2\left(9A\left(3k_1\delta\right) - A\left(k_1\delta\right)\right)}\end{aligned} \tag{12}$$

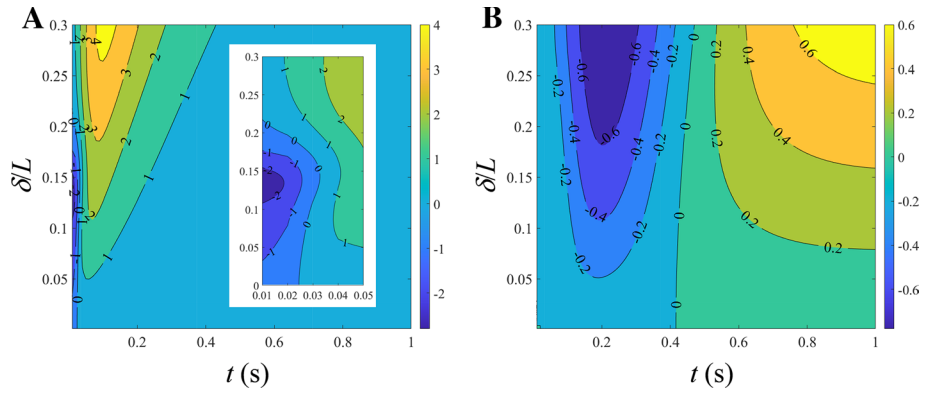

Fig. 4 Contour plots of derivative of $T_{\mathrm{pd}}(x,t)$ with respect to the horizon size δ: **a** at $x = 1.1875$ cm, and **b** at $x = 5.0$ cm

Therefore, we have theoretically shown that when t is sufficiently large, δ-convergence is monotonic in the case of 1D transient diffusion with Dirichlet boundary conditions imposed via the fictitious node mirror-type method.

When t is close to the initial time, the sign of the derivative in Eq. (8) may depend on the horizon size and δ-convergence may not be monotonic. In Fig. 4, we plot this derivative for two locations on the 1D bar: $x=1.1875$ cm (close to where a Dirichlet condition is imposed), and $x=5.0$ cm (the middle of the bar). These results confirm that when t is large, the derivative is positive (Eq. (12)). Figure 4 also reveals that at some time instant, the derivative may change sign when varying the horizon size, e.g., at $x=1.1875$ cm, when $t=0.02$ s (see Fig. 4a) or at $x=5.0$ cm, when $t=0.42$ s (see Fig. 4b).

In the discrete version, numerical and discretization errors may affect monotonicity of δ-convergence of PD solutions to the classical one, and this is discussed next. In the next section, we also see how monotonicity of δ-convergence leads to different intersection property of m-convergence curves in the PD numerical computations for transient heat transfer.

3 The Intersection of *m*-Convergence Curves at the Exact Classical Solution Value

To discretize the PD model for the 1D case, we use a uniform grid for a bar of length L, and, for the spatial integration, we employ the one-point Gauss quadrature rule (the midpoint integration). Let the grid spacing be Δx. Non-uniform grids are possible in discretizing the PD equations (see [26, 30, 31]) but this is not pursued here. The nodes at the ends of the bar have the coordinates $\Delta x/2$ and $L-\Delta x/2$, and all nodes have the same volume (length), Δx (see Fig. 2). More details on the numerical implementation are available in [19, 20, 32, 33].

We implement the three ways of imposing in the PD model the Dirichlet boundary conditions shown in Fig. 2. We first consider the mirror type, for which the PD analytical solution is available (see last section). For the 1D case shown in the last section, we showed that the PD solution converges to the corresponding classical solution when the horizon size decays to zero, and that δ-convergence may or may not be monotonic, depending on the time and location investigated (see Fig. 4). As shown in Fig. 4, for location $x=5.0$ cm, the derivative of $T_{\text{pd}}(x,t)$ with respect to the horizon size δ is negative at $t=0.3$ s, is positive

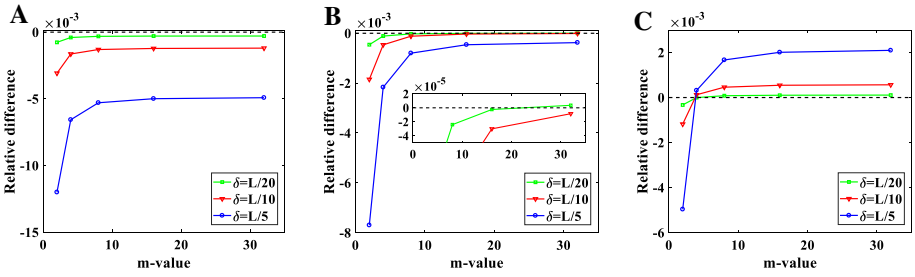

Fig. 5 Relative differences between PD solutions and the classical one for m-convergence curves of numerical PD solutions at $x=5.0$ cm with boundary conditions implemented with the mirror-type fictitious node method. **a** $t=0.3$ s; **b** $t=0.42$ s; **c** $t=0.5$ s. Time step used is $\Delta t=5\times10^{-5}$ s

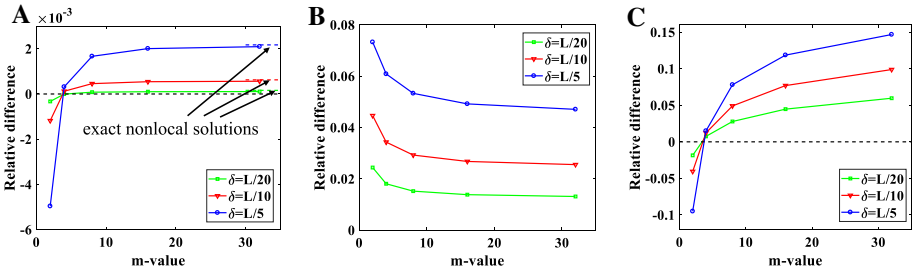

Fig. 6 m-convergence curves of PD model at $x=5.0$ cm, $t=0.5$ s, with different types of boundary conditions: **a** mirror type, **b** naïve type, and **c** inner type. Time step used is $\Delta t = 5 \times 10^{-5}$ s

at $t=0.5$ s, and at $t=0.42$ s, is close to zero, with its sign changing even for small horizon sizes. These features explain the observed different intersection properties for the m-convergence curves in the numerical PD solutions, as shown in Fig. 5.

As can be observed from Figs. 5 and 6a, the PD numerical solution converges to the corresponding analytical nonlocal solution when m goes to infinity. In Fig. 6a, the analytical PD solution values are also shown. At $t=0.3$ s (Fig. 5a), the exact PD solutions are below the classical one, consistent with the negative sign of $\frac{\partial T_{\text{pd}}(x,t)}{\partial \delta}$. At $t=0.5$ s (Fig. 5c), the exact PD solutions are above the classical one, consistent with the positive sign of $\frac{\partial T_{\text{pd}}(x,t)}{\partial \delta}$. At $t=0.42$ s (Fig. 5b), $\frac{\partial T_{\text{pd}}(x,t)}{\partial \delta}$ is close to zero, and its sign changes, depending on the horizon size, which means that the exact PD solution may be above or below the classical solution, and this is why the intersecting property of the m-curves may not happen. Note that at $t=0.5$ s (Fig. 5c), the δ-convergence for small m-values is monotonic, and approaches the classical value from below. This is induced by the discretization error, which likely "shifts" the zero level set in Fig. 4b to the right, making the derivative of the numerically obtained $T_{\text{pd}}(x,t)$ negative. The convergence then is from below, instead of from above. As m increases, one approaches the exact nonlocal solutions, for which the convergence (at the specified time and place) is from above (see Fig. 4b). This switch of "direction" of convergence, leads to the intersection of the m-curves, which, to preserve the monotonicity of δ-convergence, need to all cross at the same m-value (for a certain time and space) and the corresponding temperature there has to be the exact classical value, otherwise we contradict δ-convergence monotonicity.

In summary, the combination of numerical approximations, and δ-convergence monotonicity can lead to the intersecting m-convergence curves. The "right" combination happens relatively rarely for the fictitious-node method mirror-type style of imposing local boundary conditions in the PD model, but is more common in the inner-type implementation of boundary conditions because the approximation error introduced by this approach of approximating the local boundary conditions is significantly "stronger" than the quadrature error in the mirror-type case. This is why, for the remained for the paper we use the inner-type method.

Note that, because in all our computational tests we used an even number of nodes, there is no node in the middle of the bar. The value for that location is computed from the average of the values at the two nearest nodes. Because of this (see also Fig. 1), the computed temperatures at the middle of the bar are smaller than the exact PD value, when m is small.

For the inner-type implementation of Dirichlet boundary conditions (fixing end nodes' temperatures, see Fig. 2c) in the PD model for transient heat diffusion problem, the behavior of the m-convergence curves was discussed in our previous work (see [13, 19]). For a fixed horizon size, the PD solution converges with m going to infinity, but it may converge to a solution different from the ones obtained with the mirror-type or naïve-type boundary conditions shown in Fig. 2a, b (see comment in paragraph above Eq. 6). If we let m to go to infinity and the horizon size to go to zero, the solution converges to the exact local solution for all three ways of implementing the local boundary conditions (see [19] and Fig. 6). The convergence behavior for a general steady-state diffusion equation was also demonstrated in [34].

To understand how the time step influences the behavior of m-convergence, we first observe that, although the parabolic-type diffusion equation induces an infinite propagation speed of perturbations [23] (boundary conditions are felt instantly over the entire domain at all times), in the discrete version, the propagation is limited by time step (Δt) and the horizon size (δ) in the PD formulation. Over one time step, a node can only affect the nodes in its family (within a distance of δ). In the PD computations, the boundary condition information "propagates" at the finite speed $\delta/\Delta t$. This effect is a computational error induced by the computational time step. In dynamic elasticity problems, for elastic wave speeds smaller than $\delta/\Delta t$, we expect to see a "fake" wave front. Although FEM discretizations of the classical heat transfer problem have the same issue, there is no peridynamic surface

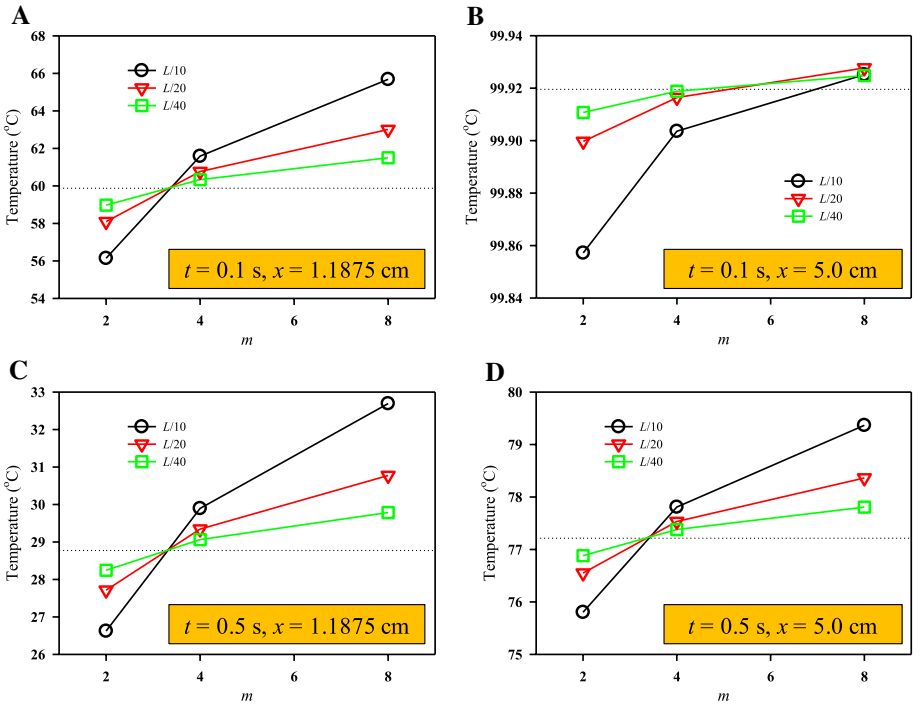

Fig. 7 The behavior of m-convergence curves at different locations in time and space for time step $\Delta t = 5 \times 10^{-5}$ s. **a** at $x = 1.1875$ cm, and $t = 0.1$ s; **b** at $x = 5.0$ cm, and $t = 0.1$ s; **c** $x = 1.1875$ cm, $t = 0.5$ s; **d** $x = 5.0$ cm, $t = 0.5$ s. Dotted lines correspond to the temperature values of the exact classical solution, respectively

effect disturbance (like there is in the inner-type implementation of local boundary conditions) to propagate through the material.

This finite propagation speed of information makes the convergence behavior depend on space and time, which means that the results in Fig. 7 in [19] showing convergence curves crossing and matching the classical temperature value at the same m value (near 3.4), would suffer if one uses, for example, a larger time step. The calculations performed in [19] used a small time step ($\Delta t = 10^{-7}$ s), selected to obtain stable PD solutions when the finest spatial grid was used ($m = 16$ and $\delta = L/160$).

In the remaining parts of this paper, we use two, relatively larger time steps 10^{-4} s and 5×10^{-5} s (for more efficient computations), to see how well the intersecting property is preserved. We impose the boundary condition (Dirichlet boundary condition) using the inner type, on the end nodes only (see Fig. 2c). We use the forward Euler method for the time integration. The smallest horizon size in this paper is $L/40$, and the largest m is 8. Thus, for the same horizon size, the finite speed in [19] is 500 or 1000 times larger than the one we compute now. In the following numerical example, we reveal how the computational error induced by the time step influences the intersection behavior of the m-convergence curves. Note that we use the temperature values (instead of relative differences to the exact classical solution) in the following convergence studies.

For each time instance, we select two locations: $x_1 = 1.1875$ cm and $x_2 = 5.0$ cm (middle of the bar). Figure 7 shows the m-convergence curves for three different horizon sizes at these locations in time and space. At 0.1 s (see Fig. 7a and b), m-convergence curves intersect at a single point for solution at location x_1, while in the middle of the bar, at x_2, the convergence curves do not intersect at the same point, and the m values of the intersection points are larger than the one at x_1. The likely explanation for the result in Fig. 7b is similar to what was observed in Fig. 5b for the case of mirror-type implementation of BCs: δ-convergence (see map in Fig. 4b), at that location and time, may not be monotonic for the inner-type method; a similar situation was noticed in Fig. 4b, where the zero level-set, by not being a vertical line, allows for the sign of the derivative of the analytical PD solution with respect to the horizon size to change sign, when the horizon changes. At 0.5 s (see Fig. 7c, d), the m-convergence curves from both locations do intersect at the classical solution, but the m value of the intersection point for x_1 location (Fig. 7c) is about 3.2, slightly smaller than the one at x_2 (Fig. 7d), which is about 3.4.

4 Obtaining the Exact Classical Solution from Several Non-Local Solutions with Large Horizons

When δ-convergence is monotonic (at a point in time and space), and for some m values the PD solution is above the classical one, while for some other is below, the m-convergence curves have to cross each other at the same m-value, and the corresponding temperature there is necessarily the exact solution of the local model (this is easily proven by contradiction, see also [19]). This leads to the potential of obtaining the exact classical solution from a number of PD solutions that employ relatively large horizons. This means also that the grids needed for these solutions are relatively coarse. A natural question is whether, with this strategy, the same m-value can be used for all points along the bar and at all times. The answer to this question was partially given in the previous section, where we observed that the crossing m-value is not necessarily constant, but that it depends on the location and

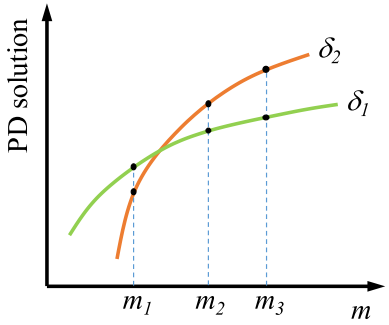

Fig. 8 Finding the intersecting m-value at the crossing point of two m-convergence curves by quadratic interpolation, from solving for the temperature at a point and time step using six different PD solutions (corresponding to given m_1, m_2, m_3, and δ_1, δ_2). Here, and in what follows, $\delta_1 = L/10$, $\delta_2 = L/20$, $m_1 = 2$, $m_2 = 4$, and $m_3 = 8$

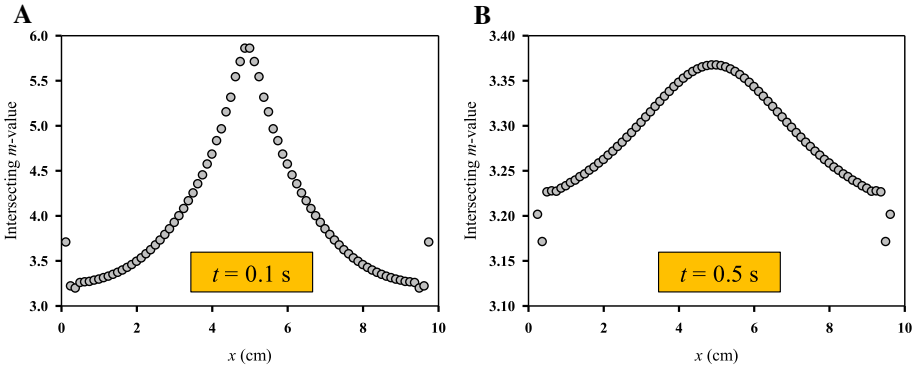

Fig. 9 Distribution of the intersecting m-values for **a** $t=0.1$ s and **b** 0.5 s. Note that the end points for $t=0.5$ s have intersecting m-values to 3.7, which are not shown in (**b**). $\Delta t = 10^{-4}$ s

time where the solution is computed. In this section we study the variation of the intersection point for m-convergence curves on the time and location along the bar, and investigate whether the proposed strategy is better than using a PD solution with a very small horizon size to approximate the exact local solution. Note that, because of δ-convergence, the PD solution with a smaller horizon size should, in principle, approximate the exact classical solution better than one obtained using with a larger horizon size.

We emphasize that, for the remainder of this paper, only the inner-type implementation of the local boundary conditions is used, because this is the more robust way to "force" m-convergence curves cross each other (at the exact classical value) at more points in space and time.

We first calculate the variation of m values at the intersection of the m-convergence curves along the 1D bar. To improve accuracy in computing the intersecting point, we interpolate three data points in the m-convergence calculations using quadratics (see Fig. 8). Note that although two quadratic curves may have two or more intersection points, we only keep the one corresponding to the smallest (but positive) m value (see Fig. 8). The desire is to choose smaller m-values because of efficiency of computations: large m-values lead to costly computations without much gain in accuracy, see the plateauing of the m-convergence curves for values of m much larger than about 8 in Figs. 5 and 6. Moreover, the key factor in getting m-convergence curves to cross is the presence of discretization error and/or of surface effects errors, and these are more prominent for smaller m-values.

This is why most of the intersecting points we found, correspond to m values between 2 and 4.

To maintain efficiency, we select two relatively-large horizon sizes: $\delta_1 = L/10$, $\delta_2 = L/20$, and for each horizon size, we use three m values: 2, 4, and 8. In Fig. 8, we schematically show the intersecting of two monotonic m-convergence curves.

With this method (see Fig. 8), we find the distribution of intersecting m-values at times 0.1 s and 0.5 s, for points along the bar, as shown in Fig. 9. These results reveal two major points:

1. The intersecting m-value for a certain point along the bar depends on the distance from the boundaries. Except for locations close to the boundaries (affected by the PD surface effect [35], present in the inner-type implementation of BCs), the m value increases as the point is further away from the boundaries. As illustrated in [19], when Dirichlet boundary conditions in Eq. (4) are imposed on the boundary nodes inside the bar (inner-type implementation, see Sect. 2), the amount of total heat present at the initial time step in the bar is lower than it should be according to the classical model; on the other hand, the nonlocality of the PD model slows the heat flow (relative to the corresponding local model), resulting in higher temperature values (or lower, depending on whether there is outflow or inflow of heat into the point) than those corresponding to the classical solution. Therefore, the earlier the boundary conditions information are felt at a point, the higher (for outflow) or lower (for inflow) the value of the numerical PD solution is, relative to the corresponding local model value. After the initial time, the intersecting m-values stay near 3.4, which is the value noted in [19] also, even though the diffusivity in this paper is different from the one in [19]. In [19], we have shown that for the linear (or "conical") micro-diffusivity in the constructive kernel, and using an asymptotically compatible quadrature scheme, δ-convergence is monotonic. Therefore, all of the results and conclusions we obtained here for the constant micro-diffusivity should also hold for the linear micro-diffusivity. In [19] we have also shown that with the linear micro-diffusivity, the intersecting m-values are slightly larger than for the constant one.
2. The intersecting m-value at particular points along the bar is not constant in time, but its variation decreases with time, tending to a constant value along the bar. With a relatively large time step, to approximate the exact solution of the classical model using the property of intersecting m-convergence curves of peridynamic models is, therefore, more efficient at the later times than at early times. At the early times, temperature changes are small and affected more strongly by the PD surface effect round-off error. As time progresses, the error will be dominated by the boundary condition implementation, which is the one canceling out the nonlocality at the intersecting point. The earlier the solution sought, the smaller the times-step used in the PD computations for finding the intersecting m-value needs to be. This seems a reasonable compromise.

We emphasize that with this strategy, using the intersecting m-value of PD solutions for two large horizons (therefore with relatively coarse corresponding grids, and therefore, at a small computational cost), we obtain the **exact** classical solution (!) at a point in time and space. In this paper, we apply this approach to compute the local solution using several PD models with large horizons with a better approximation than by using a PD solution with a smaller horizon size. This approach could be especially useful for problems with damage or other singularities.

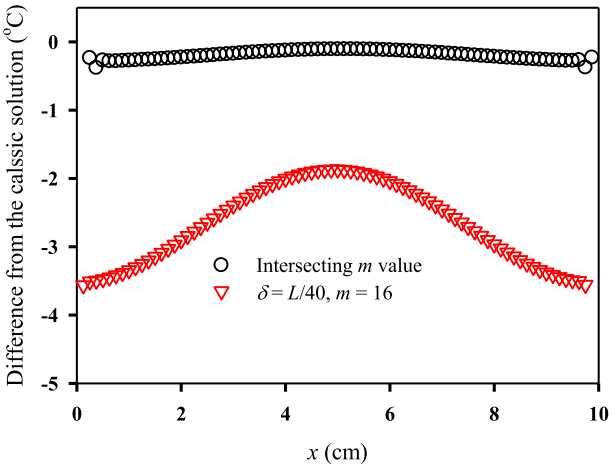

Fig. 10 The difference between the PD computed solution and the exact classical solution at time $t = 0.5$ s and $x = 5.0$ cm. The black circle data is computed based on the intersecting m-value strategy: $m = 3.367$, obtained from intersecting curves for horizon sizes $L/10$ and $L/20$. The total nodes number is 80 (corresponding to the horizon size $L/23.76$). The triangle data is based on a single PD solution with horizon size $L/40$ and $m = 16$ (total nodes number is 640). $\Delta t = 10^{-4}$ s

Next we show the effectiveness of using the intersecting m-value strategy (with two relatively large horizons) versus using the PD solution with a relatively smaller horizon to compute an approximation of the exact solution of the classical model. In the intersecting m-value strategy, we use a point at a certain time ($x_2 = 5.0$ cm and $t = 0.5$ s in Fig. 9, for instance) to find the intersecting m-value. Then, we use this m-value, and the corresponding number of nodes, to calculate the PD solution at all points along bar, at this time-step.

Figure 10 shows the difference between the PD computed solutions and the exact classical solutions. The black circles represent the results from the intersecting m-value strategy. For these results, first, we use horizon sizes: $\delta_1 = L/10$, $\delta_2 = L/20$, and for each horizon size, we select three m values: 2, 4 and 8. With each combination of horizon size and m value, we calculate the temperature value at the middle of the bar and time 0.5 s. We interpolate these solution data points using quadratic functions (as shown in Fig. 8). The crossing point of the two interpolated curves is the intersecting m-value, which is 3.367 in the case shown in Fig. 10. With this m value and a total nodes number 80, we run the PD simulation again to obtain the results at all points along the bar at time $t = 0.5$ s. The difference compared with the exact classical solution are shown as black circles in Fig. 10. We then also use a smaller horizon size and finer grid ($L/40$ and $m = 16$) to find the solution along the bar at the same time. The red triangles in Fig. 10 represent the difference between these results and the exact classical solution. Note that if the solution is needed at an earlier time, one needs to use a smaller time step in order to employ the intersecting m-value approach.

The small difference distribution between PD solution with intersecting m-value and the classical solution shown in Fig. 10 demonstrates that PD computational method can be used to obtain the classical solution. Notably, the total computational time for all PD runs based on the intersection m-value strategy involved in finding the results shown in Fig. 10 is only 1/4 of the computation time for the single PD solution with the smaller horizon size. A smaller time step would further reduce the variation in the distribution of intersecting m-values (see Fig. 9), which will further improve the results (smaller difference through the bar in Fig. 10).

Note that except for points very close to the boundary, which are directly affected by the PD surface effect, we can choose other location to determine the intersecting m-values, as long as the diffusion time is sufficiently large, or the time-step size is sufficiently small (see Fig. 9). Certainly, with different choices of location, the intersecting m-values may fluctuate more or less, and so would the approximation of the classical solutions. However, these fluctuations should be small.

The intersection property of the m-convergence curves depends in a major way on the monotonicity of δ-convergence, the numerical quadrature scheme, and the way local boundary conditions are imposed. If monotonic δ-convergence holds, then m-convergence curves either do not cross, or they all cross at a single point, whose value may or may not be equal to the classical solution value (see the cases with other postulated kernels in [19]). For a constructive kernel ($n=2$ in Eq. (1)), if monotonic δ-convergence holds and the numerical quadrature scheme is an asymptotically compatible one, then the m-convergence curves either do not cross each other or the classical solution, or they all cross at a single point and that point is the classical solution.

We have discussed in detail the monotonicity of δ-convergence for the 1D transient diffusion with Dirichlet boundary condition imposed via the three strategies discussed in Sects. 2 and 3. For higher dimensional cases and problems with other types of boundary conditions, we can apply a similar procedure to that shown in Sect. 2 for finding the analytical solutions to PD models (see [22]). Then, such analytical solutions can be used to analyze the monotonicity of the δ-convergence behavior. If δ-convergence is monotonic and the numerical quadrature scheme is asymptotically compatible, similar features as the intersection of m-convergence curves at classical solution values should persist, and one should be able to extend the methodology shown here to the higher dimensional cases and problems with other types of boundary conditions. This will be investigated in the future.

It is important to observe that in many works [18, 28, 35], PD solutions have been compared with the exact classical ones and, when a close match was observed for a certain m-value (for example, $m=3$), the conclusion was that numerical convergence has been achieved. The results presented here explain one possible reason for the nonlocal solutions obtained in such cases being very close to the exact solution: the m-value used in such cases was probably close to the intersecting point of the m-convergence curves. Had a larger m-value been used in those problems, it is likely that one would have noticed the PD solution starting to depart from the classical one.

5 The case of 1D Transient Heat Transfer in a Heterogeneous Bar

In the last section, we focused on 1D transient heat transfer in a homogeneous bar, and we explained how the intersecting m-value depends on spatial location and time/time-step. In this section, we consider transient heat transfer in a 1D heterogeneous bar and analyze whether and how material interfaces affect the intersecting property of the m-convergence curves.

We consider the bar of length, initial, and boundary conditions the same as in the homogeneous case (see Sect. 2). Two material phases are included in this heterogeneous bar. One phase (Material F, from "fast") is the same as the one used in the homogeneous case, the other (Material S, from "slow") has a diffusivity a tenth of material F's. To determine the properties of bonds crossing material interfaces, we use the harmonic average of the materials properties for the bonds crossing interfaces. To account for the portion of an

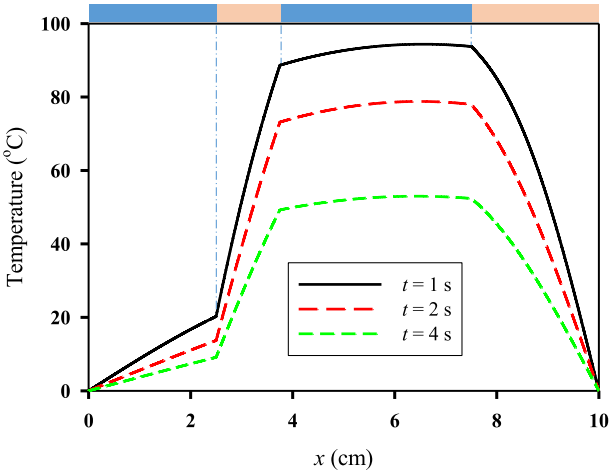

Fig. 11 FEM-computed time-evolution of temperature distribution along a 1D heterogeneous bar subject to Dirichlet boundary conditions. The different material phases (with high/orange and low/blue diffusivities) are shown at the top of the plot

interface bond belonging to each phase, we can use the area-weighted harmonic average, introduced in [36]. Other nonlocal interface (NLI) models, e.g., the new energy-based NLI model in [37], are possible. In this paper, for simplicity, we use the simple harmonic average. The bar is composed of 4 segments (see Fig. 11), with the following distribution of phases: $L/4$ (Segment 1, material F), $L/8$ (Segment 2, material S), $3L/8$ (Segment 3, material F) and $L/4$ (Segment 4, material S). Figure 11 shows the classical solution from a FEM simulation (using 1D linear truss elements, with 1280 nodes and time step 0.001 s), at $t=1$ s, 2 s, and 4 s. Obvious slope changes are observed at the phase interfaces. We next perform a convergence study for the PD corresponding model and analyze the intersection of the m-convergence curves at $t=2$ s for different points along the bar. The selection of this time is arbitrary.

The m-convergence curves for three different horizon sizes are shown in Fig. 12. Several observation locations are selected. As seen from Fig. 12, material interfaces affect the intersection of m-convergence curves. At locations close to the material interfaces, and especially for points far from the boundaries, the m-convergence curves for this time and with a time step of $\Delta t = 5 \times 10^{-5}$ s do not all intersect at a single point (see Fig. 12b, d). The m-convergence curves intersect at different m values in different segments divided by the material boundary (see Fig. 12a, c and e–h), and the intersection points may not be the same as the value from the exact classical solution (see Fig. 12e, F). Note that in Fig. 12, we simply connect the points with straight lines. For computing the intersection points, we use the quadratic interpolation as shown in Fig. 8.

In Fig. 13a, we show the distribution of m values of the m-convergence curves intersection points along the heterogeneous bar. For each material point on the bar, we interpolate two m-convergence curves by quadratic interpolation, with the same strategy as the one in Fig. 8. Since not all m-convergence curves meet at the same point (see Fig. 12), the intersecting m-value depends on which two m-convergence curves we select. However, all of the intersection points are close to the classical solution, as shown in Fig. 12. Since our aim is to compute the cheapest nonlocal models to approximate the exact solution of the classical model, for computational efficiency we select two larger horizon sizes: $\delta_1 = L/10$, $\delta_2 = L/20$, and for each horizon size, we use three m values: 2, 4 and 8.

Fig. 12 The m-convergence curves of PD solutions for transient heat transfer in a heterogeneous bar at $t=2$ s and at different locations along the bar (marked in *red* on the *bar*). In phase F (*blue*): **a** $x=1.1875$ cm, **c** $x=3.125$ cm, **e** $x=5.0$ cm, and **f** $x=6.25$ cm. In phase S (*orange*): **b** $x=2.75$ cm, close to an interface, **d** $x=3.625$ cm, close to an interface; **g** $x=8.125$ cm, and **h** $x=8.75$ cm. The *dotted lines* correspond to the FEM-computed classical solution values. $\Delta t = 5 \times 10^{-5}$ s (Color figure online) ▶

Similar conclusions as those drawn from the results in Fig. 12 can be made from the results in Fig. 13a: the intersection behavior of the m-convergence curves is influenced by the time it takes to propagate the information (including the PD surface effects) from the boundaries. Moreover, in the heterogeneous case, the presence of the material interfaces also modifies the intersecting m-values. Two other observations are: 1) as in the homogeneous case (see Fig. 9), zones farther away from the boundaries have higher m values; and 2) intersecting m-values jump at the material interfaces. For a homogeneous bar, the diffusivity value has no effect on the intersecting m-value. In the heterogeneous case, the observed jump in the intersecting m-value at an interface is likely due to the discontinuity in the effective diffusivity in the PD nonlocal model and the selection for deciding bond properties for PD bonds that cross a material interface. The area-weighted harmonic average introduced in [36] may be used to mitigate the effect from the jump discontinuity in the material properties, but it is not pursued in this work. It might also be possible to develop an approach similar to the fictitious nodes method for material interfaces, which could also improve on the results shown here.

In Fig. 13b, we use the intersecting m-value at $x=5.0$ cm and $t=2$ s ($m=4.432$) from Fig. 13a, and a relative grid-density with the total nodes number 160, and we show the difference between the PD computational solution and the FEM solution. The intersecting m-value approach has a smaller difference to the classical (FEM-based) solution than the PD solution obtained with a single, but much smaller horizon size. In the future, it will be interesting to investigate whether for problems with singularities in the classical solution, the intersecting m-value can be more efficient even than a FEM-computed solution.

6 Concluding Remarks

In this paper we analyzed the behavior of peridynamic (PD) numerical solutions for transient heat/mass diffusion subject to Dirichlet boundary conditions. We investigated whether a strategy based on intersecting m-convergence curves that compute several PD solution using large horizons leads to better/more effective approximations of the exact solution of the classical model than a single PD model that uses a much smaller horizon size.

We have clearly explained the source for the intersecting m-convergence curves by using analytical solutions to PD models of transient heat transfer and the numerical approximations of various ways of imposing local boundary conditions, in the context of the one-point Gaussian spatial quadrature (mid-point integration).

With the one-point Gauss quadrature and an appropriate peridynamic kernel, numerical results converge to the classical solution in the limit of the horizon going to zero when the relative grid-density (m) is kept constant. The intersection of m-convergence curves at the classical solution is due to the competition between numerical discretization effects and the way of implementing the local boundary conditions and the nonlocality present in a PD model. We noticed that the behavior of m-convergence curves intersecting at the classic solution provides a better approximation of the exact classical solution that using a PD model with a smaller horizon size. It is therefore possible to find a certain m-value for

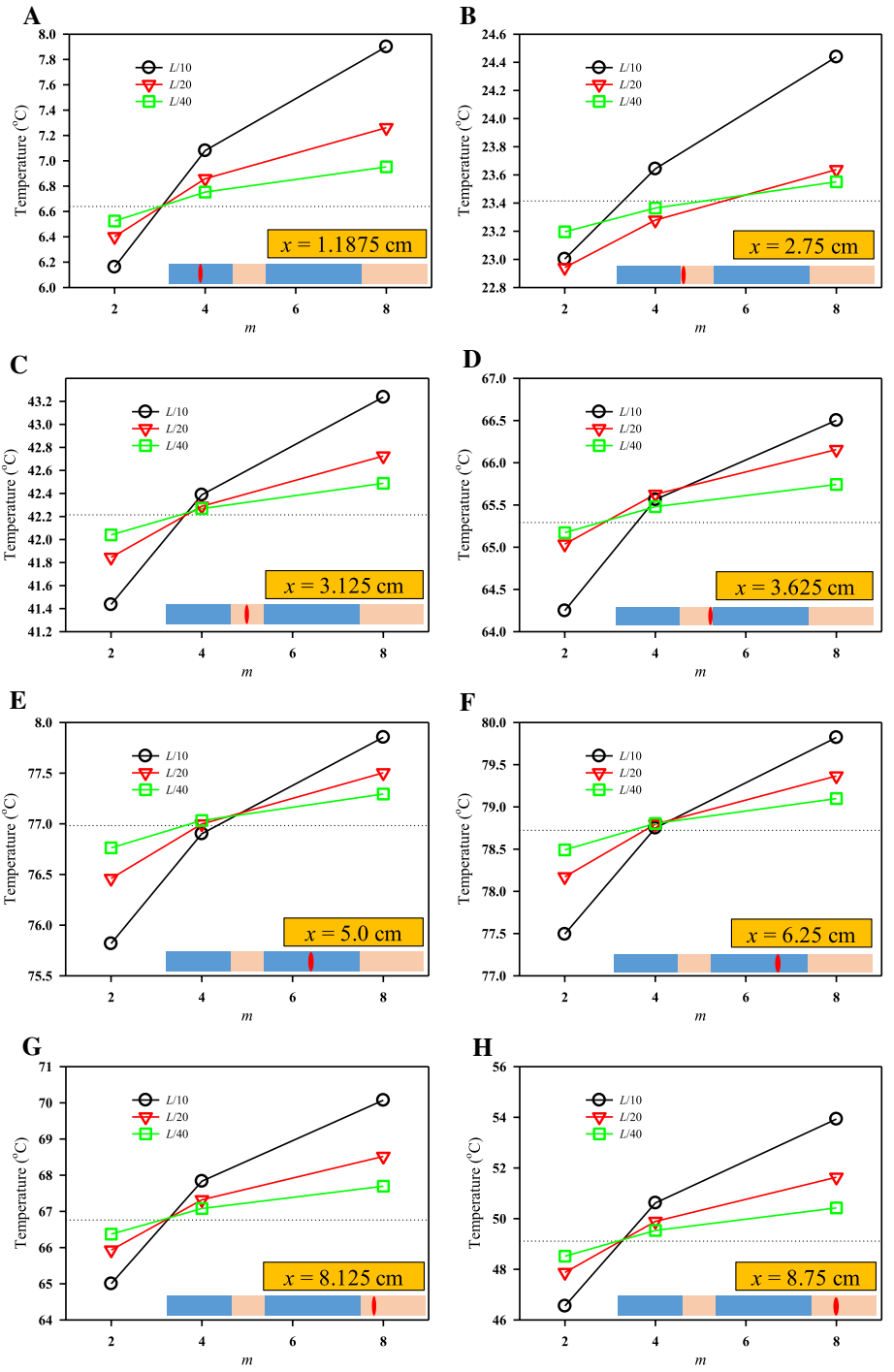
A
B
C
D
E
F
G
H
L/10
L/20
L/40
Temperature (°C)
m
x = 1.1875 cm
x = 2.75 cm
x = 3.125 cm
x = 3.625 cm
x = 5.0 cm
x = 6.25 cm
x = 8.125 cm
x = 8.75 cm

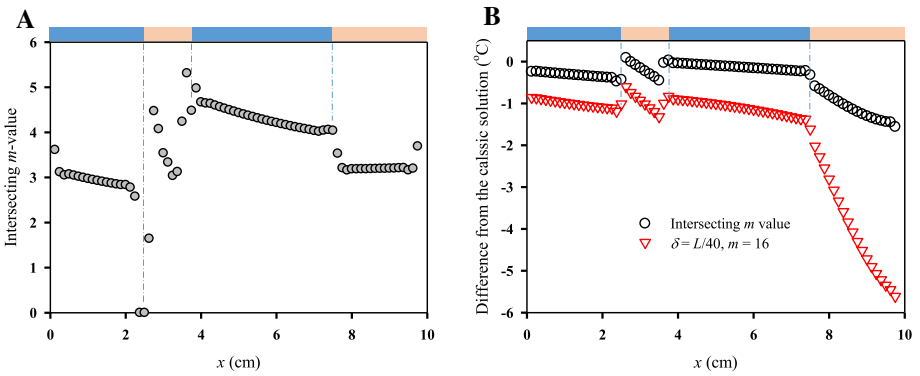

Fig. 13 Heat transfer in a heterogeneous bar. **a** Distribution of the intersecting m-values for $t=2$ s. Note that if the intersection point is outside the region of $m \in (0, 8)$, we set the m value as zero. **b** The difference between the PD computational solution and the FEM solution of 1D heat transient in a heterogeneous bar at time $t=2$ s. Black circles: fixed m value selected at $x=5.0$ cm and $t=2$ s in (**a**), and the total nodes number is 160 (corresponding to horizon size $L/36.1$). *Red inverted triangles*: using horizon size is $L/40$ and $m=16$ (total nodes number is 640). Time step used in PD tests: $\Delta t = 10^{-4}$ s (Color figure online)

which, even with a large nonlocal size, one finds the exact local solution at a point in time and space.

We also performed convergence studies for 1D transient heat transfer in a composite bar made of alternative phases with high and low diffusivities. We showed that material interfaces have a strong influence on the m-convergence intersection points value for the solution at different locations along the bar. The benefits observed for the homogeneous bar are maintained for the heterogeneous bar: m-convergence curves for peridynamic solutions obtained with different horizon sizes cross at the classical solutions, when an "asymptotically compatible" numerical scheme is used.

Note that the properties discussed here were obtained for the one-point Gaussian quadrature (meshfree PD implementation). They may persist for other types of discretization methods, but we have not studied that so far.

Acknowledgements This work was supported by the Natural Science Foundation of China (No. 11802098) and the Natural Science Foundation of Hubei Province (No. 2018CFB111). The work of F.B. and J. Z. was supported by the US National Science Foundation CMMI CDS&E Grant No. 1953346 (program manager Joanne Culbertson). The authors would like to thank the anonymous reviewers for constructive comments and suggestions that have led to significant improvements.

Declarations

Conflict of interest The authorsdeclare that they have no competing interests.

References

1. Luciani, J.F., Mora, P., Virmont, J.: Nonlocal heat-transport due to steep temperature-gradients. Phys. Rev. Lett. **51**(18), 1664–1667 (1983)
2. Mahan, G.D., Claro, F.: Nonlocal theory of thermal-conductivity. Phys. Rev. B **38**(3), 1963–1969 (1988)

3. Sobolev, S.L.: Equations of transfer in nonlocal media. Int. J. Heat Mass Transfer **37**(14), 2175–2182 (1994)
4. Grmela, M., Lebon, G.: Finite-speed propagation of heat: a nonlocal and nonlinear approach. Phys. A **248**(3–4), 428–441 (1998)
5. Chen, G.: Ballistic-diffusive equations for transient heat conduction from nano to macroscales. J. Heat Transfer **124**(2), 320–328 (2002)
6. Alvarez, F.X., Jou, D.: Memory and nonlocal effects in heat transport: From diffusive to ballistic regimes. Appl. Phys. Lett. **90**(8), 083109 (2007)
7. Tzou, D.Y., Guo, Z.Y.: Nonlocal behavior in thermal lagging. Int. J. Therm. Sci. **49**(7), 1133–1137 (2010)
8. Yu, Y.J., Tian, X.G., Xiong, Q.L.: Nonlocal thermoelasticity based on nonlocal heat conduction and nonlocal elasticity. Eur. J. Mech. A Solids. **60**, 238–253 (2016)
9. Silling, S.A.: Reformulation of elasticity theory for discontinuities and long-range forces. J. Mech. Phys. Solids. **48**(1), 175–209 (2000)
10. Silling, S.A., Epton, M., Weckner, O., Xu, J., Askari, E.: Peridynamic states and constitutive modeling. J. Elasticity **88**(2), 151–184 (2007)
11. Cheng, Z.Q., Fu, Z.Q., Zhang, Y., Wu, H.X.: A peridynamic model for analyzing fracture behavior of functionally graded materials used as an interlayer. Acta Mech. Solida Sin. **33**, 781–792 (2020)
12. Gerstle, W., Silling, S., Read, D., Tewary, V., Lehoucq, R.: Peridynamic simulation of electromigration. Comput. Mater. Con. **8**(2), 75–92 (2008)
13. Bobaru, F., Duangpanya, M.: The peridynamic formulation for transient heat conduction. Int. J. Heat Mass Transfer **53**(19–20), 4047–4059 (2010)
14. Bobaru, F., Duangpanya, M.: A peridynamic formulation for transient heat conduction in bodies with evolving discontinuities. J. Comput. Phys. **231**(7), 2764–2785 (2012)
15. Du, Q., Gunzburger, M., Lehoucq, R.B., Zhou, K.: Analysis and approximation of nonlocal diffusion problems with volume constraints. SIAM Rev. **54**(4), 667–696 (2012)
16. Tian, X., Du, Q.: Analysis and comparison of different approximations to nonlocal diffusion and linear peridynamic equations. SIAM J. Numer. Anal. **51**(6), 3458–3482 (2013)
17. Wang, L.J., Xu, J.F., Wang, J.X.: A peridynamic framework and simulation of non-fourier and nonlocal heat conduction. Int. J. Heat Mass Transfer **118**, 1284–1292 (2018)
18. Oterkus, S., Madenci, E., Agwai, A.: Fully coupled peridynamic thermomechanics. J. Mech. Phys. Solids. **64**, 1–23 (2014)
19. Chen, Z.G., Bobaru, F.: Selecting the kernel in a peridynamic formulation: a study for transient heat diffusion. Comput. Phys. Commun. **197**, 51–60 (2015)
20. Chen, Z.G., Bakenhus, D., Bobaru, F.: A constructive peridynamic kernel for elasticity. Comput. Methods Appl. Mech. Eng. **311**, 356–373 (2016)
21. Hu, W.K., Wang, Y.N., Yu, J., Yen, C.F., Bobaru, F.: Impact damage on a thin glass plate with a thin polycarbonate backing. Int. J. Impact Eng. **62**, 152–165 (2013)
22. Chen, Z., Peng, X., Jafarzadeh, S., Bobaru, F.: Analytical solutions of peridynamic equations. Part I: transient heat diffusion. (In preparation)
23. Evans, L.C.: Partial differential equations. American Mathematical Society, Rhode Island (2010)
24. Rosenau, P.: Tempered diffusion: a transport process with propagating fronts and inertial delay. Phys. Rev. A **46**(12), R7371 (1992)
25. Andreu, F., Caselles, V., Mazon, J.M., Moll, S.: Finite propagation speed for limited flux diffusion equations. Arch. Ration. Mech. Anal. **182**(2), 269–297 (2006)
26. Bobaru, F., Ha, Y.D.: Adaptive refinement and multiscale modeling in 2D peridynamics. Int. J. Multiscale Comput. Eng. **9**(6), 635–659 (2011)
27. Katiyar, A., Foster, J.T., Ouchi, H., Sharma, M.M.: A peridynamic formulation of pressure driven convective fluid transport in porous media. J. Comput. Phys. **261**, 209–229 (2014)
28. Oterkus, S., Madenci, E., Agwai, A.: Peridynamic thermal diffusion. J. Comput. Phys. **265**, 71–96 (2014)
29. Kreyszig, E.: Advanced Engineering Mathematics. John Wiley and Sons, London (2017)
30. Li, S.M., Chen, Z.G., Tan, L., Bobaru, F.: Corrosion-induced embrittlement in ZK60A Mg alloy. Mat. Sci. Eng. A Struct. **713**, 7–17 (2018)
31. Henke, S.F., Shanbhag, S.: Mesh sensitivity in peridynamic simulations. Comput. Phys. Commun. **185**(1), 181–193 (2014)
32. Zhao, J.M., Chen, Z.G., Mehrmashhadi, J., Bobaru, F.: Construction of a peridynamic model for transient advection-diffusion problems. Int. J. Heat Mass Transfer **126**, 1253–1266 (2018)

33. Zhao, J.M., Jafarzadeh, S., Chen, Z., Bobaru, F.: An algorithm for imposing local boundary conditions in peridynamic models of diffusion on arbitrary domains. (under review). https://doi.org/https://doi.org/10.31224/osf.io/7z8qr
34. Tian, X.C., Du, Q.: Asymptotically compatible schemes and applications to robust discretization of nonlocal models. SIAM J. Numer. Anal. **52**(4), 1641–1665 (2014)
35. Le, Q., Bobaru, F.: Surface corrections for peridynamic models in elasticity and fracture. Comput. Mech. **61**(4), 499–518 (2018)
36. Mehrmashhadi, J., Tang, Y.Y., Zhao, X.L., Xu, Z.P., Pan, J.J., Le, Q.V., Bobaru, F.: The effect of solder joint microstructure on the drop test failure-a peridynamic analysis. IEEE T. Comp. Pack. Man. **9**(1), 58–71 (2019)
37. Capodaglio, G., D'Elia, M., Bochev, P., Gunzburger, M.: An energy-based coupling approach to nonlocal interface problems. Comput. Fluids **207**, 104593 (2020)